Materials and Design 181 (2019) 108084

Contents lists available at ScienceDirect

Materials and Design

journal homepage: www.elsevier.com/locate/matdes

Critical assessment of high speed nanoindentation mapping technique and data deconvolution on thermal barrier coatings

B. Vignesh [a], W.C. Oliver [b], G. Siva Kumar [a], P. Sudharshan Phani [a,*]

[a] International Advanced Research Centre for Powder Metallurgy & New Materials (ARCI), Balapur P.O., Hyderabad, Telangana 500005, India
[b] Nanomechanics Inc., 105 Meco Ln, Oak Ridge, TN 37830, USA

HIGHLIGHTS

- Assessment of high speed nanoindentation mapping technique on a complex material system such as thermal barrier coating
- Identification of phases, microstructural features and interfaces from the property map and comparison with microstructure
- Deconvolution based on k-means clustering to obtain phase level properties and construction of mechanical phase maps
- Effect of thermal cycling on microstructural, compositional and mechanical property changes of individual phases

GRAPHICAL ABSTRACT

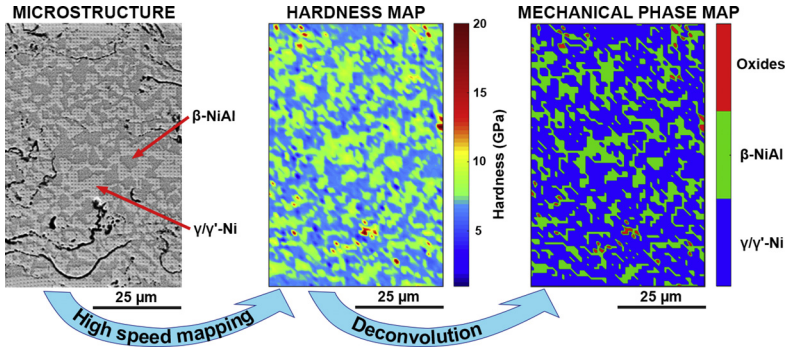

ARTICLE INFO

Article history:
Received 6 June 2019
Received in revised form 25 July 2019
Accepted 29 July 2019
Available online 30 July 2019

Keywords:
Thermal barrier coating
Nanoindentation
Mapping
Deconvolution
Thermally grown oxide

Data availability:
The raw/processed data required to reproduce these findings cannot be shared at this time due to technical or time limitations.

ABSTRACT

A critical assessment of the high speed nanoindentation technique is performed by testing a complex material system such as thermal barrier coating (TBC). Extensive nanoindentation tests are performed to spatially map the properties of bond coat, top coat and bond coat-top coat interface regions of as-coated and thermally cycled TBCs and the resulting spatial property maps (hardness and elastic modulus maps) are compared with the corresponding microstructures to establish correlations. Excellent correlation is observed between the microstructure and the mechanical properties at the micrometer length scale. The various microstructural features and phases including thermally grown oxide (TGO) at the bond coat-top coat interface are accurately captured by the mapping technique. A deconvolution technique based on k-means data clustering algorithm is used to obtain the phase level properties from the maps and also generate mechanical phase maps to visualize the evolution of mechanical properties with thermal cycling which enables a holistic understanding of degradation mechanisms operating at various levels of thermal cycling. The capabilities of the high speed nanoindentation mapping demonstrated in this work have important implications for microstructure based finite element modeling and also for development of data-driven models for predicting the life of TBCs.

1. Introduction

High speed nanoindentation mapping is emerging as an advanced nanomechanical characterization tool to study the local mechanical response of multi-phase materials. With better electronics and novel

* Corresponding author.
E-mail address: spphani@arci.res.in (P.S. Phani).

https://doi.org/10.1016/j.matdes.2019.108084

mechanical design, it is now possible to perform indentation tests much faster (~1 s per indent) than ever before. This enables performing large number of indentation tests in the specific region of interest within a short duration of time which results in the spatial mapping of the material properties. Each indent in the array provides local information on the mechanical property of the small volume of material that is being probed beneath the indenter. This massive dataset of highly localized (micron scale) mechanical properties can be of great use to study the linkages between the microstructural features and its corresponding properties such as hardness and elastic modulus. On the other hand, the large experimental data thus generated allows for conducting advanced statistical data analysis of the results. So far, high speed nanoindentation mapping technique has been reported by several groups on cementitious materials [1–4], cermets [5], composites [6,7], nanolaminate carbide [8], Bakken Shale [9,10] (sedimentary rocks) and biological samples such as wood cell [11], teeth enamel [12], etc. However, mapping studies on a complex system such as thermal barrier coating (TBC) where the coating failure greatly depends on the evolution of local mechanical properties of the various layers during operation are very limited [13].

TBCs are multi-layer, multi-material systems that are provided for the thermal insulation and oxidation resistance of the underlying structural components [14]. It typically consists of an intermetallic bond coat which are usually MCrAlY alloys where M = Ni or Co or both, a porous ceramic top coat such as yttria stabilized zirconia (YSZ) and a thermally grown oxide (TGO) layer that forms at the interface between bond coat and top coat as a result of high temperature operation. To add to the complexity, different microstructural features such as the splat boundaries for thermal sprayed coatings, porosity, interface between layers, cracks, etc., co-exists in TBCs. Moreover, as these coatings are usually subjected to extreme environments, material degradation such as aluminum depletion in bond coat, growth of TGO at bond coat-top coat interface, densification of top coat, etc., takes place with time and temperature [15]. While in operation, these degradation mechanisms can operate simultaneously and cause changes in its microstructure and/or composition [16].

Given the complexities inherent to TBC systems and the advantages of an emerging technique such as high speed mapping, there exist a strong case to apply these techniques for studying TBCs. Doing so, enables the study of the spatial and temporal variations in properties of different layers of TBCs. If successful, such a study can provide structure-property correlation at the micron scale which can be used to understand the performance of the coating. In addition, this can also help in understanding the effect of material degradation mechanisms on the mechanical properties and provide better insights about the failure of these coatings.

Such a study has two primary requirements viz., a high-speed technique to perform large number of indentation tests in a relatively short time span and a data deconvolution technique to statistically analyze the data and retrieve quantitative information from indentation tests. Data deconvolution can be performed in different ways. For instance, Constantinides et al. [17], assumed the data to follow multi-modal Gaussian distribution and performed deconvolution by fitting its probability distribution function. Later, Ulm et al. [18] used cumulative distribution for fitting, to overcome the limitations of fitting probability distribution function. Recently, Veytskin et al. [19] used Gaussian mixture deconvolution by expectation maximization technique. Although these techniques provide a quantitative estimate of the properties of individual phases, they have two major drawbacks — (1) the need to assume a certain distribution for the data (Gaussian, Lorentzian, etc.) and (2) loss of spatial information of the constituents, wherein, an average value for each phase is estimated without any regard to its spatial coordinates. Also, most of the previous work [20–24] on mapping of local mechanical properties of TBCs has been limited to layer level averaged response and restricted to fewer tests, precluding any rigorous statistical treatment.

The ability to track and analyze the phase level properties has direct implications for materials design [25]. The measurement of mechanical properties of different phases (within each layer of TBC) with change in material composition and operating conditions, serves as a valuable input for microstructure based modeling tool [26] such as Object Oriented Finite element analysis, where feeding phase level properties could improve the accuracy of the model.

In view of these potential advantages, the capabilities of the high speed mapping technique are assessed by testing a complex material system like TBC. In addition to the insights to the thermal spray community, using a TBC to assess the high speed mapping technique, enables testing the applicability of the technique on samples with significant porosity, significant topographic changes, multiple phases with different sizes and morphologies, multiple interfaces (layer to layer, particle to particle, etc.) and multiple material types (metals, intermetallics, ceramics, etc.). In this regard, high speed nanoindentation mapping has been performed to spatially map the bond coat, top coat and the interface regions of TBCs subjected to different levels of thermal cycling. The resulting property maps are compared with the microstructure to establish correlations. A novel methodology based on k-means data clustering algorithm is used for deconvoluting mapping data to obtain properties of constituent phases without loss of spatial information. The evolution of microstructure and there by the properties during thermal cycling of the entire TBC system enables a holistic understanding of the degradation mechanisms leading to coating failure.

2. Materials and methods

2.1. Coating deposition

Thermal barrier coatings with NiCoCrAlY bond coat and YSZ top coat have been investigated in this study. Both, bond coat and top coat was deposited using Atmospheric plasma spray coating facility carrying a 9 MB (Sulzer Metco, Switzerland) spraying gun. The substrate is a 10 × 10 × 5 mm flat rectangular specimen of Ni-based super alloy (C263). The substrate was grit blasted prior to coating deposition in order to improve the adhesion of the coating. The bond coat was subsequently overlaid on this roughened substrate. The feedstock powder used was Amperit 47.05Ni-23Co-17Cr-12.5Al-0.45Y (wt%), with a particle size range of 22–45 μm. YSZ containing 7 wt% Y_2O_3 (Amperit) with a particle size range of 10–45 μm was then overlaid on top of the bond coat. The average bond coat and top coat thickness is 105 μm and 175 μm, respectively.

2.2. Thermal cycling

The coated samples were subjected to thermal cycling which is one of the most widely used accelerated tests to assess the lifetime of TBCs. Thermal cycling in the present study involves heating the samples to 1100 °C in 20 min, holding at 1100 °C for 40 min and cooling to 300 °C within 10 min. This was carried out using a thermal cycling furnace (CM Furnaces-Bloomfield, USA) which can be automated to perform the thermal cycling to desired number of cycles. Samples were drawn after 5, 10, 50 and 100 cycles for mechanical and microstructural characterization.

2.3. Sample preparation

The thermally cycled samples were initially cold mounted using epoxy resin in order to prevent potential damage during cutting operations for cross sectional studies. The samples were then sheared using abrasive wheel cutter (Isomet, Buehler, USA) to expose the cross section of the sample. The cross sectional surface was hot mounted using bakelite powder for further polishing operations. The cross section was polished with abrasive SiC papers of increasing grit size (1000, 2000 & 4000). Finally, the samples were subjected to vibratory polishing in a

60 nm colloidal silica solution using Vibromet2 (Buehler, USA) for 2 h. Obtaining a polished surface with minimal damage due to the polishing process is critical for high speed nanoindentation mapping. While the extent of polishing damage cannot be easily estimated, special care was taken, especially during the initial stages of polishing where coarse grits were used, to gently polish and minimize the extent of damage.

2.4. High speed nanoindentation mapping

Nanoindentation testing was carried out using an iNano® nanoindenter manufactured by Nanomechanics Inc., (a KLA Tencor company, Oak Ridge, TN, USA). A diamond Berkovich tip (E = 1141 GPa; $\nu = 0.07$) was used for all the tests. Nanoblitz3D®, a high speed mapping technique, wherein each indent typically takes less than a second, was used for mapping. This includes the time taken for surface approach, surface detection, loading, unloading and positioning the sample for next indentation. This revolutionary improvement in terms of instrumentation and the recent advancement in the understanding of theoretical basis for minimum indentation spacing [27], enables high speed-high resolution spatial mapping over large areas (typically 1000's μm^2) with thousands of indents. Maps of different sizes (typically containing more than 10,000 indents) were carried out on the bond coat, top coat and bond coat-top coat interface regions of as-coated and thermally cycled samples. After performing area function calibration on fused silica samples and correcting for load-frame compliance, the hardness and elastic modulus for every indent was calculated using standard Oliver & Pharr method [28]. The indentation load was accordingly chosen to ensure a minimum indent spacing to indent depth ratio of 10 based on the recent work of Sudharshan Phani et al. [27]. The maximum depth of indentation was largely dictated by the tradeoff between the lower signal-to-noise at smaller depths and lower resolution of the maps at higher depths (or indent spacing). While a thorough theoretical treatment on the maximum depth of indentation to capture the intrinsic properties is challenging, simple trial and error type experimental study was carried out to determine an optimal maximum depth to capture the intrinsic properties of the various features of the TBCs. Thus, all tests were performed to a maximum load of 2 mN (which results in <100 nm depth) with 1 μm spacing between the indents (i.e., at least 10 times the depth). In all, 212,500 indents were performed to map the as-coated and thermally cycled samples for obtaining structure-property correlations at the micrometer length scale and also for subsequent statistical analysis.

2.5. Microstructural characterization

The nanoindentation maps were imaged using a Scanning Electron Microscope (Hitachi-S3400N, Japan). Bond coat and bond coat-top coat interface maps were captured in Back Scattered Electron (BSE) mode. Energy Dispersion Spectroscopy (EDS) spot analysis was performed on different phases present in the samples to determine the composition of the constituent phases. An optical microscope (Olympus, Japan) was also used to image the coatings, especially in the porous top coat region.

2.6. Data deconvolution

In the present work, data deconvolution involves determining the properties of individual phases from the spatial property map of a multi-phase specimen. A data clustering algorithm called k-means was used for this purpose. The algorithm used is similar to the one described elsewhere [29]. The primary function of k-means is to partition '*n*' observations into '*k*' clusters. K-means is an iterative refinement technique which initializes k cluster centers at random and minimizes the intra-cluster sum of squares of distances in each iteration, by shifting the position of cluster centers to a new point. This iterative process converges when the intra-cluster distances can no more be reduced, thereby separating the data into a predetermined number of clusters. The number of clusters into which the data has to be binned can be determined either by prior knowledge of the number of phases present in the mapped region, or by iteratively running the algorithm for different number of clusters and picking the optimal number by error minimization. As the algorithm partitions the data in such a way that the data points within the same cluster are more similar than those in other clusters, it is expected that each cluster represents a distinct phase/feature in the spatial map. Once clustered, the mean and standard deviation of the data points in each cluster can be used as a quantitative measure of the property of the corresponding phase. This method of deconvolution has been applied to all spatial property maps acquired from bond coat, top coat and bond coat-top coat interface regions to obtain the properties of individual phases/features (β-

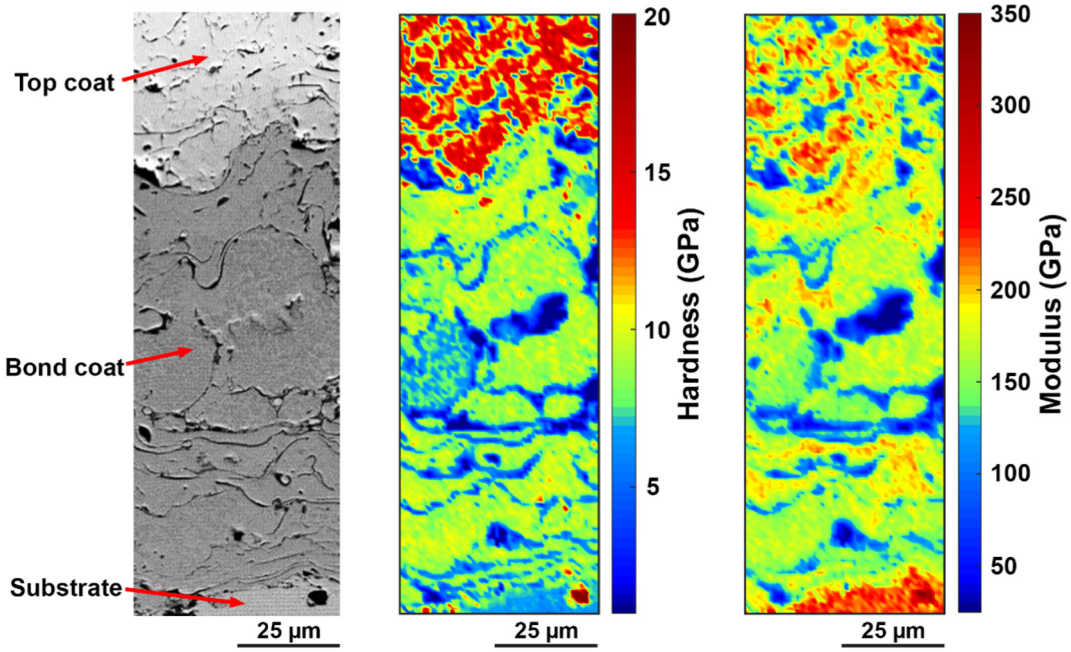

Fig. 1. Cross-sectional SEM micrograph and the corresponding hardness and elastic modulus map of an as-coated TBC showing different coating layers.

NiAl, γ/γ′-Ni, YSZ, TGO) present in them. It is worth noting that, unlike the Gaussian deconvolution-based methods, this method retains the spatial information of the various constituent phases, which is useful for studying the evolution of local mechanical property.

3. Results and discussion

The spatial property maps of the bond coat, bond coat-top coat interface and top coat regions of as-coated and thermally cycled TBCs are presented in Section 3.1. Application of data deconvolution algorithm on these maps and the effect of thermal cycling on the hardness and elastic modulus of different phases in the TBCs are presented in Section 3.2.

3.1. Microstructure-property correlation

Fig. 1 shows the microstructure, hardness and elastic modulus map of the cross-section of the TBC in the as-coated state. The map covers $50 \times 150\ \mu m^2$ area comprising of 7500 indents. The hardness and elastic modulus variation across different layers and also within each layer is clearly captured by the maps indicating that the indent spacing is sufficient to capture the key microstructural features. This also demonstrates that the technique is capable of handling abrupt changes in properties and topography that result while mapping across the layers and across splat boundaries or pores that are typical of thermal sprayed coatings. A detailed analysis of the spatial property variation within each layer and its evolution with thermal cycling is presented in the following subsections.

3.1.1. Bond coat

The microstructure, hardness and elastic modulus maps of the bond coat in the as-coated and thermally cycled states are shown in Fig. 2. The splat boundaries are very distinct in the as-coated state (Fig. 2a), which is typical of plasma sprayed coatings. The hardness in the as-coated state is higher than that of the thermally cycled ones. In contrast, the elastic modulus shows the opposite effect with thermal cycling. The differences in the hardness and elastic modulus with thermal cycling can

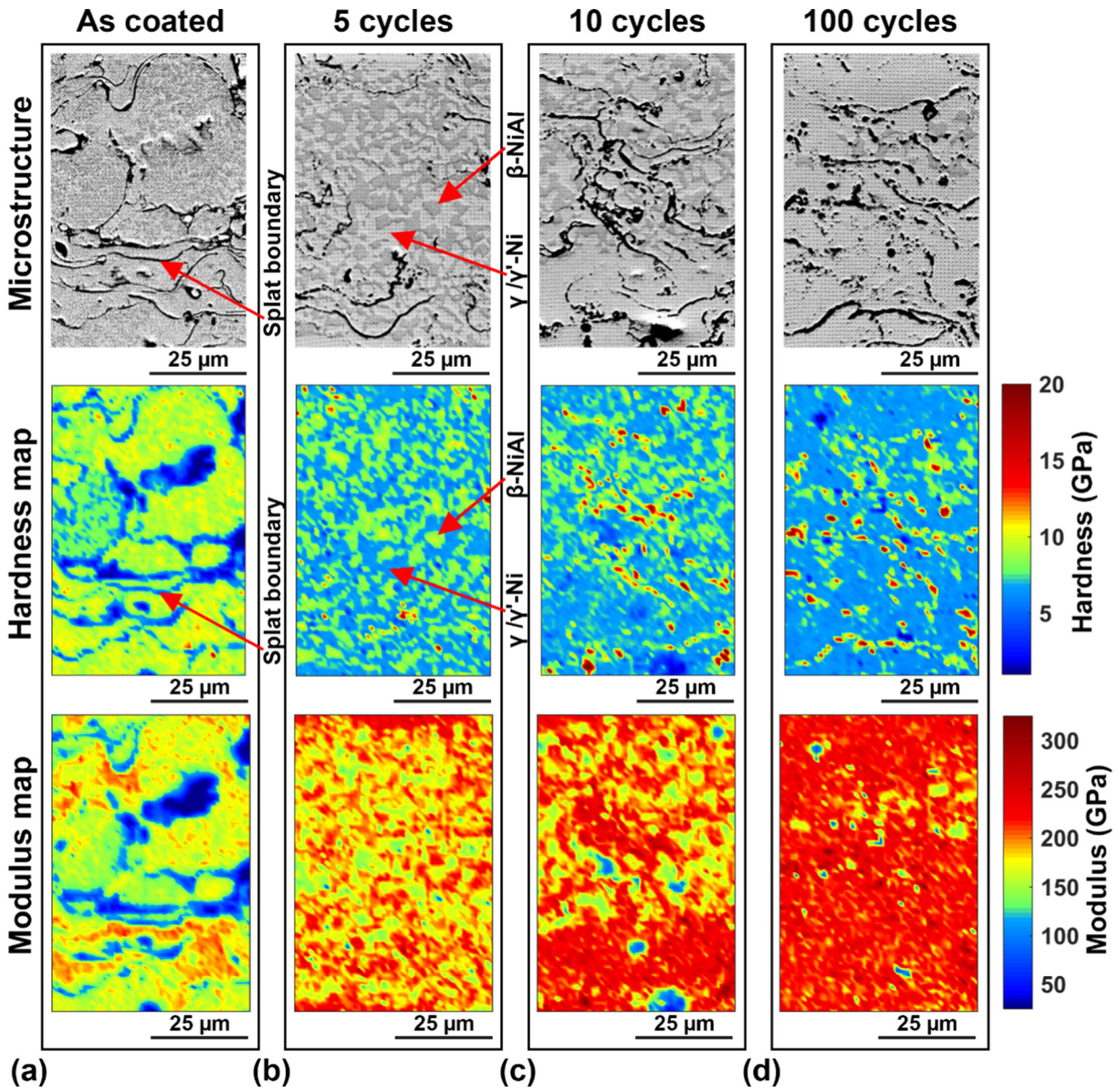

Fig. 2. Cross-sectional SEM micrographs and the corresponding hardness and elastic modulus maps of NiCoCrAlY bond coat in (a) as-coated state and after (b) 5 (c) 10 and (d) 100 thermal cycles, respectively.

be attributed to the microstructural changes that can be observed from the SEM micrographs.

In the case of sample subjected to 5 thermal cycles shown in Fig. 2b, a two phase microstructure can be observed. The darker shade of gray corresponds to the β-NiAl phase and the lighter shade is the γ/γ′-Ni matrix. This was verified through aluminum content determined through EDS and is similar to the observations of Hemker et al. [30] with the β-NiAl regions being relatively large and inter-connected at this state. A comparison of the microstructure and hardness map of the sample subjected to 5 thermal cycles shows excellent correlation, wherein the property variation and morphology of the two phases has been precisely captured. The β-NiAl phase is harder than the γ/γ′-Ni phase, while the elastic modulus shows an opposite trend. The BCC like arrangement in the β-NiAl can result in the higher hardness compared to the FCC γ/γ′-Ni. A comparison of the microstructure in the as-coated state and after 5 thermal cycles shows that the splat boundaries have significantly healed. Upon close observation of the hardness map after 5 thermal cycles, a few regions/spots with very high hardness can be observed. EDS analysis on such spots indicate that they are most likely Al rich oxides which are known to form due to internal oxidation of the bond coat [31]. The results for the sample subjected to 10 thermal cycles are shown in Fig. 2c. A comparison of its microstructure with the sample subjected to 5 cycles, shows that the relative area fraction of β-NiAl decreases which is clearly captured in the hardness map. The hardness map also shows an increase in the fraction of the high hardness regions, which indicates that the area fraction of the oxides has increased with thermal cycling. With further thermal cycling up to 100 cycles (Fig. 2d), the β-NiAl phase is almost depleted and the fraction of the oxides increases further. Interestingly, the hardness map also shows that the oxides are found preferentially at the splat boundaries. The property maps after 50 thermal cycles are similar to the ones after 100 cycles and hence are not shown here. In summary, the hardness maps and to a certain extent the elastic modulus maps, show excellent correlation with the microstructure and are able to accurately capture the microstructural changes at the micrometer length scale.

3.1.2. Bond coat-top coat interface

The bond coat-top coat interface is one of the most critical regions of a TBC. The major microstructural and the corresponding mechanical property variations during operation, occur in this region. This ultimately has a bearing on the thermal cyclic life of the TBC. The most significant event at the bond coat-top coat interface is the formation of a thermally grown oxide (TGO) layer [32]. TGO forms due to a reaction between inter-diffused aluminum (from the β-NiAl of bond coat) with the ingressive oxygen (through top coat) at high temperature. A dense, contiguous layer of TGO, having a parabolic growth rate is known to prevent further oxidation of the bond coat and the underlying substrate. However, beyond a certain critical thickness, this layer causes severe strain incompatibilities and mismatch stresses, causing TBCs to damage progressively and delaminate ultimately [33,34]. Hence, determining the local elastic modulus in the TGO is extremely valuable. However, given that the desirable TGO thickness is typically of the orders of few microns, there has been no reliable local mechanical property measurement, while it is sandwiched between the bond coat and top coat. The high speed mapping at the micron length scale demonstrated in the case of bond coat makes it now possible to measure the properties of the TGO.

The microstructure, hardness and elastic modulus map around the bond coat-top coat interface in the as-coated state and after thermal cycling are shown in Fig. 3. The interface shows undulations which is

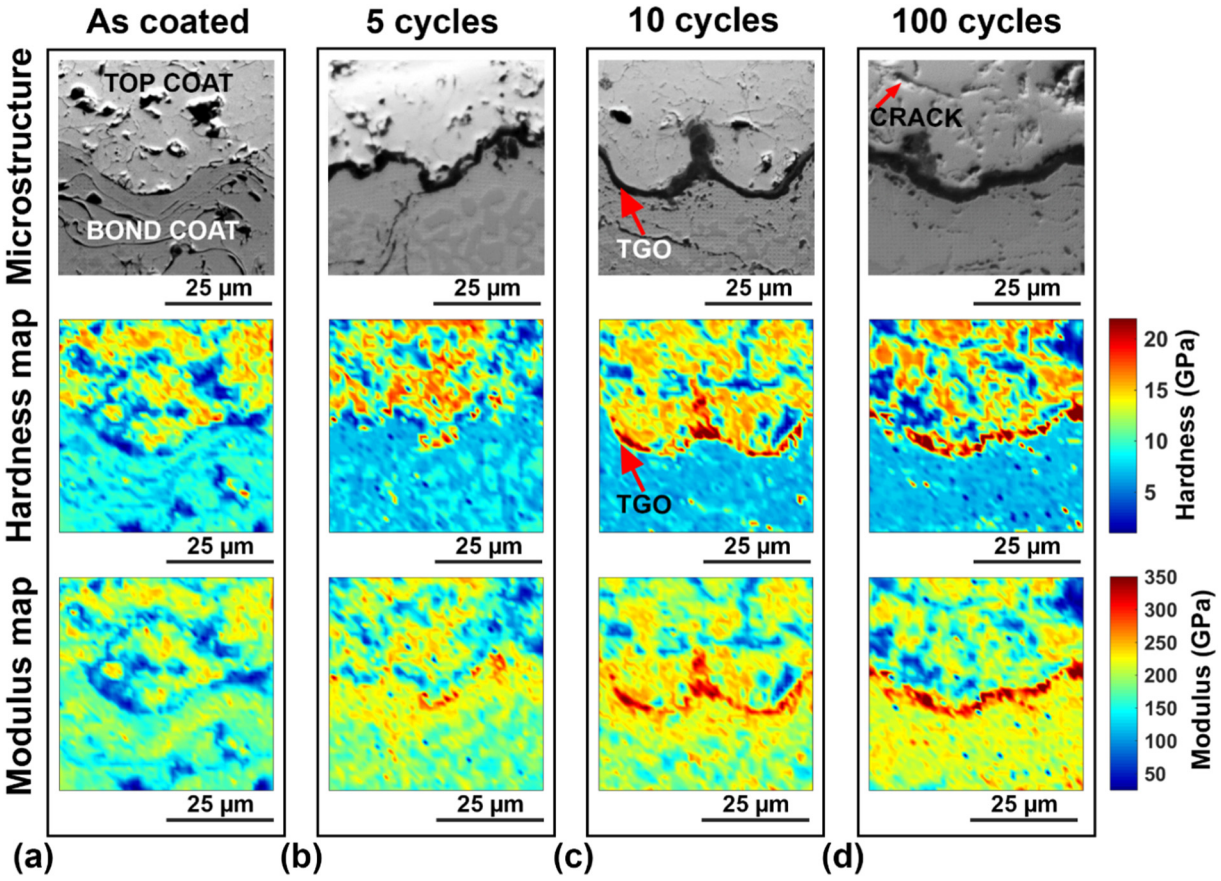

Fig. 3. Cross-sectional SEM micrographs and the corresponding hardness and elastic modulus maps at the bond coat-top coat interface in the (a) as-coated state and after (b) 5 (c) 10 and (d) 100 thermal cycles, respectively, showing the TGO growth.

typical of plasma spray coatings. A comparison of the microstructure of the as-coated and thermally cycled samples shows that the TGO (dark region at the interface) can be observed starting from 5 cycles and the thickness of the TGO increases with thermal cycling. The corresponding hardness and elastic modulus maps show a similar trend, wherein the TGO can be identified by the higher hardness and elastic modulus regions at the interface. Interestingly, the thickness of the TGO measured from the maps shows a parabolic behavior which has been observed from the microstructural studies in the past [22,35]. In addition to the growth of TGO with increasing number of thermal cycles, the depletion of the β-NiAl phase, which acts as an aluminum source on the bond coat side, can be clearly observed from the hardness maps and the microstructure.

As mentioned earlier, the difference in elastic modulus due to the growth of the TGO is one of the primary driving forces for the development of mismatch stresses. This leads to the generation of microcracks in top coat just above the interface as shown in Fig. 3d, for the case of the sample subjected to 100 thermal cycles. The reduction in the hardness and elastic modulus in the cracked regions is also captured by the maps. In summary, the high speed mapping technique can be used to measure the local mechanical properties at the interface of different layers of a coating and for the specific case of a bond coat-top coat interface of a TBC, this technique enables measurement of local elastic properties which can be readily used in FEA for simulating delamination of TBCs subjected to thermal cycling.

3.1.3. Top coat

The microstructure, hardness and elastic modulus map of the top coat in the as-coated state and after thermal cycling are shown in Fig. 4. From the microstructure it is evident that it is highly porous, which can potentially cause difficulties in high speed mapping. However, the property maps shown in the figure indicate that the mapping technique is capable of dealing with the large topographic and property variation due to the pores. Excellent correlation can be observed between the microstructure and the property for all the samples, with the porous regions exhibiting lower hardness and elastic modulus. The hardness and elastic modulus of the top coat remains constant with thermal cycling at the cycled temperatures and time scales studied in the present work. Quantifying the volume fraction of the pores either through micrographs or through maps, was not straightforward due to the ambiguity in distinguishing between the pores due to coating deposition and the pull outs due to subsequent polishing of the sample before testing.

3.2. Data deconvolution to determine properties of individual phases

The correlation between the microstructure and the property maps presented in Section 3.1 is visually apparent, but not quantitative. In order to determine phase level information of the mechanical properties of the various layers in the TBC, the high speed mapping data has to be deconvoluted. The various statistical techniques available for this purpose have been described in Section 2.6. As mentioned earlier, unlike the traditional methods that typically involve curve fitting assuming that the data follows a Gaussian or a Lorentzian distribution, a clustering algorithm is used in the present work that does not need any such assumption and also retains the spatial information about the phases after deconvolution. This enables reconstructing a phase map from the mechanical property map. Also, the clustering algorithm does not

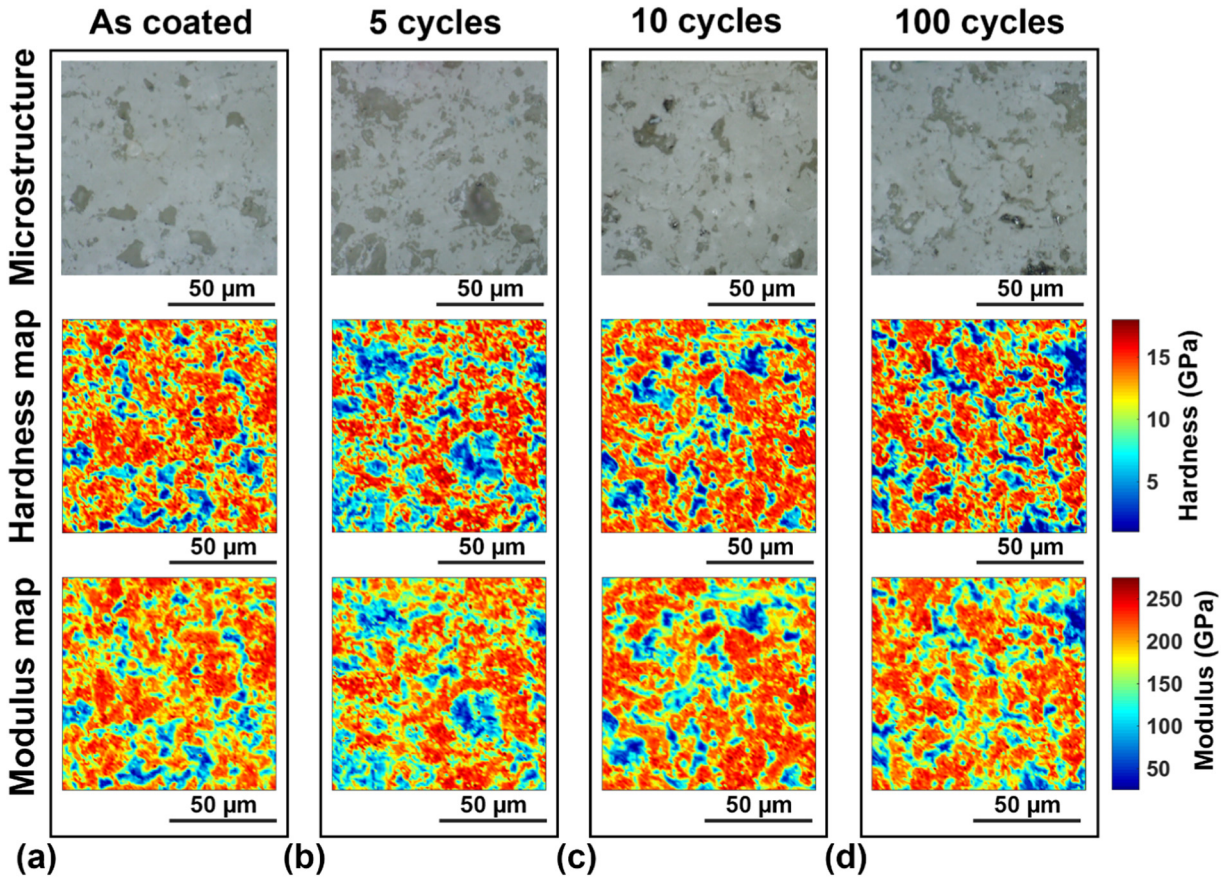

Fig. 4. Cross-sectional optical micrographs and the corresponding hardness and elastic modulus maps of the YSZ top coat in the (a) as-coated state and after (b) 5 (c) 10 and (d) 100 thermal cycles, respectively.

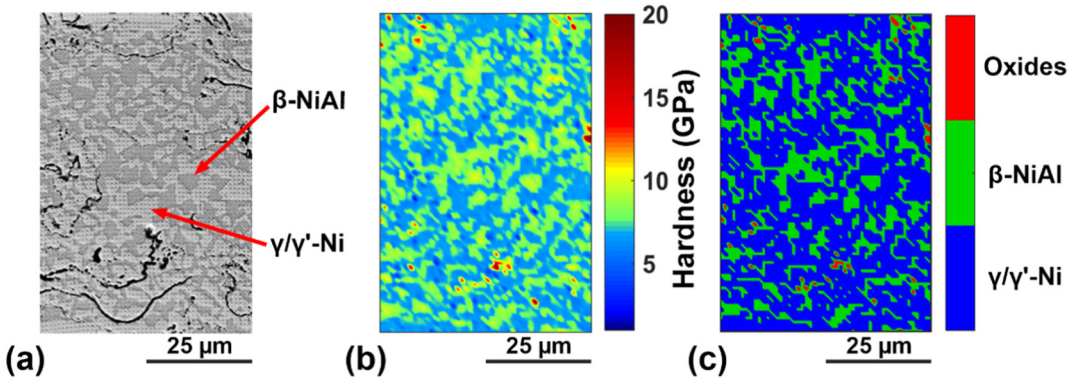

Fig. 5. (a) Microstructure and (b) hardness map and (c) deconvoluted hardness map of bond coat after 5 thermal cycles.

require any initial guess or expected range of the output which are typically required for curve fitting procedures. A deconvoluted map obtained from the hardness map along with the microstructure for the case of a sample subjected to 5 thermal cycles is shown in Fig. 5. It can be seen from Fig. 5c that the property map shown in Fig. 5b, has been separated into three distinct clusters based on the hardness data, which in this case are β-NiAl, γ/γ′-Ni and oxides due to internal oxidation. The mean and standard deviation of the data points in each cluster can be assumed to represent the mean and standard deviation of the corresponding phases as discussed in Section 2.6. A close comparison of the microstructure (Fig. 5a) and the corresponding deconvoluted map (Fig. 5c) shows that there is excellent agreement in the size and shape of the microstructural features shown in the microstructure and deconvoluted map. This also enables accurate estimation of the area fractions of the phases from the deconvoluted map, which is obtained by taking the ratio of the number of data points in a cluster to the total number of points.

Similar deconvolution procedure was applied for bond coats subjected to different thermal cycles and the deconvoluted maps are shown in Fig. 6. Note that an additional cluster has been used to identify the splat boundaries in the case of as-coated samples and are denoted as pores in the deconvoluted map. The deconvoluted maps at different thermal cycling states very clearly show the microstructural evolution, with the β-NiAl dominated microstructure in the as-coated state to γ/γ′-Ni dominated microstructure after 100 thermal cycles due to aluminum depletion. Also, the fraction of the oxides increases with thermal cycling as shown in Fig. 7. While, these observations can also be made from hardness maps, deconvolution enables quantitative results in addition to being a valuable tool for visualization.

The hardness and elastic modulus of the individual phases in the bond coat and top coat including the TGO, determined from the deconvolution is shown in Fig. 8. As expected, γ/γ′-Ni is the softest phase followed by β-NiAl and the hardness decreases for these phases upto 5 thermal cycles and remains constant thereafter. Ni enrichment due to the transformation of β-NiAl with thermal cycling is expected to decrease the hardness. Also, the nano Ni_3Al precipitates coherently distributed in the γ/γ′-Ni are reported to coarsen with thermal cycling [30]. Interestingly, these effects do not result in any significant change in hardness. In the case of YSZ, hardness remains constant with cycling, as it is known to be stable at the thermal cycling temperatures and time scales tested in this work [36]. The hardness of TGO slightly increases with cycling. However, the increase in the mean value is not significant compared to the standard deviation.

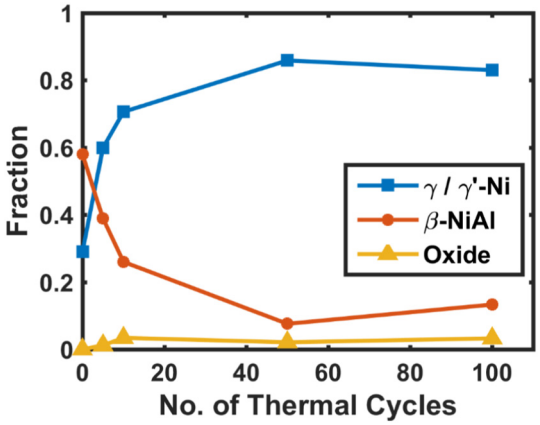

Fig. 7. Phase fraction determined from deconvolution of hardness map as a function of number of thermal cycles.

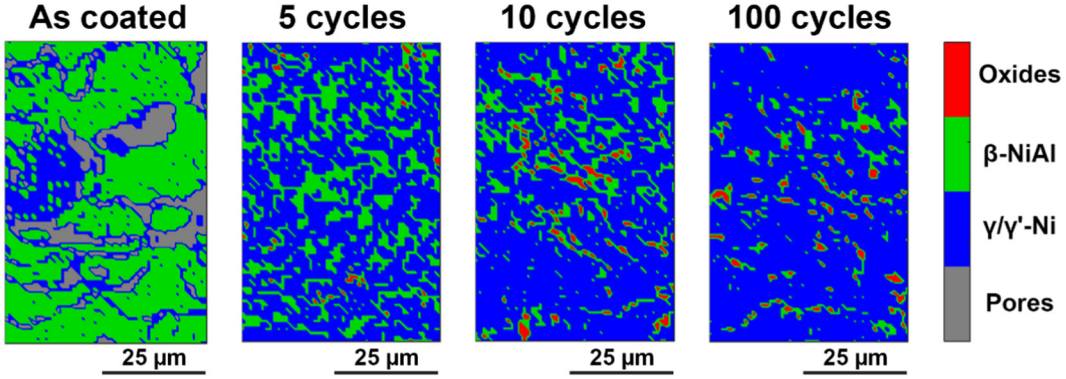

Fig. 6. Deconvoluted maps of bond coat at various levels of thermal cycling.

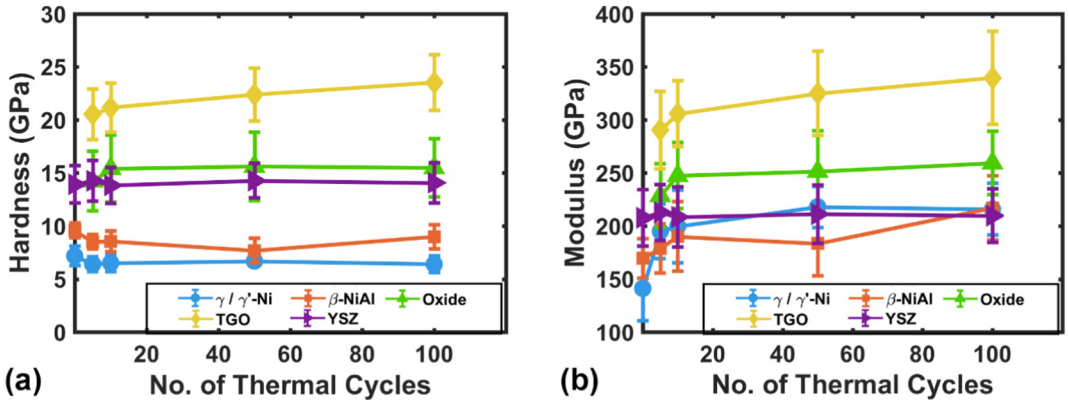

Fig. 8. (a) Hardness and (b) elastic modulus determined from deconvolution as a function of number of thermal cycles for the various phases in the TBC.

In contrast to the results for hardness, elastic modulus (Fig. 8b) of the phases in the bond coat shows an increase in the case of 5 cycles compared to the as-coated state without much change thereafter. While the elastic modulus of YSZ remains constant with thermal cycling as was the case with hardness, the elastic modulus of TGO increases with cycling. This could be due to compositional change of the oxide, especially with the changing Al content with thermal cycling. Also, the relatively smaller size of the TGO in the beginning may have resulted in measuring the combined effect of the TGO and the surrounding bond coat or top coat and hence the properties of the TGO may be treated as apparent properties and may not be intrinsic properties. The hardness and elastic modulus of the individual phases thus determined are also in general agreement with the reported values in literature [21,22], which are mostly based on a small number of indentation tests. Table 1 summarizes the hardness and elastic modulus of the various phases determined from high speed mapping and data deconvolution. The values obtained from conventional nanoindentation testing at comparable depths are also shown for comparison. Good agreement between the mapping results and the conventional indentation results can be observed for all the layers at different cycling conditions. A few discrepancies are observed but are well within the experimental scatter that can be expected in such systems. This could also be due to the fact that the conventional tests are not specifically targeted to land on a particular phase/feature. In summary, these results validate the accuracy of the high speed mapping technique on a complex material system like TBCs.

4. Implications for design

The capabilities of high speed property mapping demonstrated in the present work have important implications for materials design. For instance, phase level properties obtained through deconvolution of high speed mapping data can readily be used as input material properties for different phases in microstructure-based modeling tools such as OOF [26]. Such models foster construction of realistic geometric representations and can precisely capture the influence of microstructure on local mechanical response of the material. These models can also be of great use for micro scale crack propagation studies wherein previous work [37] has shown that the crack driving force is greatly dependent on the microstructure and its corresponding local mechanical properties. Furthermore, high resolution spatial mapping capability can be utilized to capture the local variations in properties induced by various non-equilibrium processes involved in additive manufacturing that result in gradients in microstructure and thereby mechanical properties [38]. The mapping capabilities coupled with deconvolution can be used to establish the linkages between the processing and local mechanical properties to ultimately help optimize the process. Similar to the TGO interface studies reported in this work, this technique can be employed to study the interface properties of composites [39], where the mechanical response of the interface between matrix and reinforcement dictates the strength of the composite material. In addition to spatial variations, temporal variation in properties due to composition gradients such as in a diffusion couple [40], can also be captured via a systematic study and can gainfully be used to study the kinetics. Moreover, though not demonstrated in the present work, this technique has the potential to capture crystal orientation specific properties [5], which helps to understand the associated anisotropic effects and provide insights for crystal plasticity finite element modeling. Finally, the high speed mapping capabilities demonstrated in this work, can be used to quickly establish structure-property linkages at micrometer length scale or higher, which can help in understanding multiscale mechanics and development of hierarchical materials [41]. This in turn expedites

Table 1
Hardness (H) and elastic modulus (E) values determined by high speed nanoindentation and conventional nanoindentation.

Sample condition	High speed nanoindentation										Conventional nanoindentation			
	γ/γ′-Ni		β-NiAl		Internal oxide		TGO		YSZ		Bond coat		Top coat	
	H	E	H	E	H	E	H	E	H	E	H	E	H	E
	GPa	GPa	GPa	GPa	GPa	GPa	GPa	GPa	GPa	GPa	GPa	GPa	GPa	GPa
As-coated	7.2 ± 0.9	141.2 ± 30.6	9.6 ± 0.7	169.6 ± 18.5	–	–	–	–	13.9 ± 1.8	207.7 ± 26.5	9.9 ± 1.0	165.9 ± 18.7	14.4 ± 3.6	206.9 ± 38.1
5 cycles	6.4 ± 0.7	195.0 ± 25.6	8.5 ± 0.7	178.8 ± 22.9	14.2 ± 2.8	228.5 ± 30.2	20.5 ± 2.4	290.4 ± 36.6	14.3 ± 1.9	212.8 ± 26.4	7.4 ± 0.4	218.5 ± 19.3	13.1 ± 4.7	193.0 ± 47.6
10 cycles	6.5 ± 0.8	199.7 ± 34.2	8.5 ± 1.0	190.1 ± 32.7	15.4 ± 3.1	247.5 ± 31.3	21.2 ± 2.3	305.7 ± 30.9	13.8 ± 1.7	208.4 ± 28.5	8.3 ± 0.9	200.8 ± 25.6	15.6 ± 2.6	207.4 ± 32.7
50 cycles	6.7 ± 0.4	218.0 ± 19.4	7.7 ± 1.2	183.5 ± 30.7	15.6 ± 3.2	251.4 ± 38.2	22.4 ± 2.5	325.1 ± 39.8	14.3 ± 1.6	211.1 ± 27.4	7.7 ± 0.6	213.1 ± 34.4	15.9 ± 2.1	227.9 ± 32.5
100 cycles	6.4 ± 0.8	215.8 ± 24.4	9.0 ± 1.1	216.9 ± 30.3	15.5 ± 2.7	259.4 ± 30.0	23.5 ± 2.6	339.6 ± 43.9	14.1 ± 1.9	209.6 ± 25.3	7.5 ± 0.4	222.7 ± 27.9	16.5 ± 2.6	230.9 ± 14.7

the development of novel materials for high performance under an Integrated Computational Material Engineering (ICME) approach.

The other important aspect of this technique is its high-throughput, which can be used to generate large data sets that can be processed using machine learning (ML) algorithms [42,43]. For instance, the local hardness and elastic modulus data for samples subjected to different thermal cycles obtained in the present work can be used to train ML algorithms. This can then be used to develop a data-driven model for predicting the residual life of thermal barrier coatings. As data science is considered as the new avenue for accelerating materials design and discovery, this technique with high-fidelity, high-throughput can greatly contribute to this new paradigm.

5. Summary and conclusions

1. High speed nanoindentation mapping has been carried out on as-coated and thermally cycled TBC comprising of plasma sprayed NiCoCrAlY bond coat and YSZ top coat on a super alloy substrate.
2. Excellent correlation was found between the microstructure and the local mechanical properties at the micrometer length scale even at the interface between the various layers of TBC and also in the porous top coat.
3. K-means clustering algorithm which retains the spatial information of the constituent phases was used to deconvolute the data to determine the phase level properties. The local mechanical properties of the different phases in the bond coat and the TGO as a function of the number of thermal cycles was determined. The high speed nanoindentation results agree well with reported literature and conventional nanoindentation measurements.
4. The phase level properties obtained from this analysis can be readily used for microstructure based finite element analysis and the large data sets obtained through extensive mapping can also be used to develop data-driven models for predicting residual life of TBCs.

CRediT authorship contribution statement

B. Vignesh: Investigation, Formal analysis, Visualization, Writing - original draft. **W.C. Oliver:**Formal analysis, Visualization, Writing - review & editing, Supervision. **G. Siva Kumar:**Investigation. **P. Sudharshan Phani:**Conceptualization, Methodology, Formal analysis, Writing - review & editing, Supervision.

References

[1] M. Sebastiani, R. Moscatelli, F. Ridi, P. Baglioni, F. Carassiti, High-resolution high-speed nanoindentation mapping of cement pastes: unravelling the effect of microstructure on the mechanical properties of hydrated phases, Mater. Des. 97 (2016) 372–380, https://doi.org/10.1016/j.matdes.2016.02.087.

[2] L. Brown, P.G. Allison, F. Sanchez, Use of nanoindentation phase characterization and homogenization to estimate the elastic modulus of heterogeneously decalcified cement pastes, Mater. Des. 142 (2018) 308–318, https://doi.org/10.1016/j.matdes.2018.01.030.

[3] L. Xu, F. Deng, Y. Chi, Nano-mechanical behavior of the interfacial transition zone between steel-polypropylene fiber and cement paste, Constr. Build. Mater. 145 (2017) 619–638, https://doi.org/10.1016/j.conbuildmat.2017.04.035.

[4] J. Xu, D.J. Corr, S.P. Shah, Nanomechanical properties of C-S-H gel/cement grain interface by using nanoindentation and modulus mapping, J. Zhejiang Univ. Sci. A 16 (2015) 38–46, https://doi.org/10.1631/jzus.a1400166.

[5] J.J. Roa, P. Sudharshan Phani, W.C. Oliver, L. Llanes, Mapping of mechanical properties at microstructural length scale in WC-Co cemented carbides: assessment of hardness and elastic modulus by means of high speed massive nanoindentation and statistical analysis, Int. J. Refract. Met. Hard Mater. 75 (2018) 211–217, https://doi.org/10.1016/j.ijrmhm.2018.04.019.

[6] E.D. Hintsala, U. Hangen, D.D. Stauffer, High-throughput nanoindentation for statistical and spatial property determination, Jom (2018) 9–12, https://doi.org/10.1007/s11837-018-2752-0.

[7] E. Koumoulos, C. Charitidis, Integrity of carbon-fibre epoxy composites through a nanomechanical mapping protocol towards quality assurance, Fibers 6 (2018) 78, https://doi.org/10.3390/fib6040078.

[8] C. Tromas, N. Ouabadi, V. Gauthier-Brunet, M. Jaouen, S. Dubois, Mechanical properties of nanolaminate Ti_3SnC_2 carbide determined by nanohardness cartography, J. Am. Ceram. Soc. 93 (2010) 330–333, https://doi.org/10.1111/j.1551-2916.2009.03412.x.

[9] K. Liu, M. Ostadhassan, B. Bubach, K. Ling, B. Tokhmechi, D. Robert, Statistical grid nanoindentation analysis to estimate macro-mechanical properties of the Bakken Shale, J. Nat. Gas Sci. Eng. 53 (2018) 181–190, https://doi.org/10.1016/j.jngse.2018.03.005.

[10] C. Li, M. Ostadhassan, A. Abarghani, A. Fogden, L. Kong, Multi-scale evaluation of mechanical properties of the Bakken shale, J. Mater. Sci. 54 (2019) 2133–2151, https://doi.org/10.1007/s10853-018-2946-4.

[11] L. Qin, L. Lin, F. Fu, M. Fan, Micromechanical properties of wood cell wall and interface compound middle lamella using quasi-static nanoindentation and dynamic modulus mapping, J. Mater. Sci. 53 (2018) 549–558, https://doi.org/10.1007/s10853-017-1185-4.

[12] J.L. Cuy, A.B. Mann, K.J. Livi, M.F. Teaford, T.P. Weihs, Nanoindentation mapping of the mechanical properties of human molar tooth enamel, Arch. Oral Biol. 47 (2002) 281–291, https://doi.org/10.1016/S0003-9969(02)00006-7.

[13] G. Bolelli, M.G. Righi, M.Z. Mughal, R. Moscatelli, O. Ligabue, N. Antolotti, M. Sebastiani, L. Lusvarghi, E. Bemporad, Damage progression in thermal barrier coating systems during thermal cycling: a nano-mechanical assessment, Mater. Des. 166 (2019), 107615. https://doi.org/10.1016/j.matdes.2019.107615.

[14] D.R. Clarke, M. Oechsner, N.P. Padture, Thermal-barrier coatings for more efficient gas-turbine engines, MRS Bull. 37 (2012) 891–898, https://doi.org/10.1557/mrs.2012.232.

[15] V. Kumar, K. Balasubramanian, Progress update on failure mechanisms of advanced thermal barrier coatings: a review, Prog. Org. Coat. 90 (2016) 54–82, https://doi.org/10.1016/j.porgcoat.2015.09.019.

[16] B.G. Mendis, B. Tryon, T.M. Pollock, K.J. Hemker, Microstructural observations of as-prepared and thermal cycled NiCoCrAlY bond coats, Surf. Coat. Technol. 201 (2006) 3918–3925, https://doi.org/10.1016/j.surfcoat.2006.07.249.

[17] G. Constantinides, K.S. Ravi Chandran, F.J. Ulm, K.J. Van Vliet, Grid indentation analysis of composite microstructure and mechanics: principles and validation, Mater. Sci. Eng. A 430 (2006) 189–202, https://doi.org/10.1016/j.msea.2006.05.125.

[18] O.J.A. Ulm Franz-Josef, Vandamme Matthieu, Bobko Chris, O.C. Tai Kuangshin, Statistical indentation techniques for hydrated nanocomposites: concrete, bone, and shale, J. Am. Ceram. Soc. 90 (2007) 2677–2692, https://doi.org/10.1111/j.1551-2916.2007.02012.x.

[19] Y.B. Veytskin, V.K. Tammina, C.P. Bobko, P.G. Hartley, M.B. Clennell, D.N. Dewhurst, R.R. Dagastine, Micromechanical characterization of shales through nanoindentation and energy dispersive X-ray spectrometry, Geomech. Energy Environ. 9 (2017) 21–35, https://doi.org/10.1016/j.gete.2016.10.004.

[20] N. Zotov, M. Bartsch, G. Eggeler, Thermal barrier coating systems — analysis of nanoindentation curves, Surf. Coat. Technol. 203 (2009) 2064–2072, https://doi.org/10.1016/j.surfcoat.2009.02.008.

[21] M. Hasegawa, Y. Kagawa, Microstructural and Mechanical Properties Changes of a NiCoCrAlY Bond Coat With Heat Exposure Time in Air, vol. 301, 2006 293–301, https://doi.org/10.1111/j.1744-7402.2006.02085.x.

[22] D.-J. Kim, Evaluation of the degradation of plasma sprayed thermal barrier coatings using nano-indentation, J. Nanosci. Nanotechnol. 9 (2011) 7271–7277, https://doi.org/10.1166/jnn.2009.1786.

[23] J.A. Thompson, T.W. Clyne, The effect of heat treatment on the stiffness of zirconia top coats in plasma-sprayed TBCs, Acta Mater. 49 (2001) 1565–1575, https://doi.org/10.1016/S1359-6454(01)00065-9.

[24] S. Nath, I. Manna, J.D. Majumdar, Nanomechanical behavior of yttria stabilized zirconia (YSZ) based thermal barrier coating nanomechanical behavior of yttria stabilized zirconia (YSZ) based thermal barrier coating, Ceram. Int. 41 (2014) 5247–5256, https://doi.org/10.1016/j.ceramint.2014.11.039.

[25] E.P. Koumoulos, S.A.M. Tofail, C. Silien, D. De Felicis, R. Moscatelli, D.A. Dragatogiannis, E. Bemporad, M. Sebastiani, C.A. Charitidis, Metrology and nanomechanical tests for nano-manufacturing and nano-bio interface: challenges & future perspectives, Mater. Des. 137 (2018) 446–462, https://doi.org/10.1016/j.matdes.2017.10.035.

[26] G. Bolelli, A. Candeli, H. Koivuluoto, L. Lusvarghi, T. Manfredini, P. Vuoristo, Microstructure-based thermo-mechanical modelling of thermal spray coatings, Mater. Des. 73 (2015) 20–34, https://doi.org/10.1016/j.matdes.2015.02.014.

[27] P. Sudharshan Phani, W.C. Oliver, A critical assessment of the effect of indentation spacing on the measurement of hardness and modulus using instrumented indentation testing, Mater. Des. 164 (2019), 107563. https://doi.org/10.1016/J.MATDES.2018.107563.

[28] W.C. Oliver, G.M. Pharr, An improved technique for determining hardness and elastic modulus using load and displacement sensing indentation experiments, J. Mater. Res. 7 (1992) 1564–1583, https://doi.org/10.1557/JMR.1992.1564.

[29] J.A. Hartigan, M.A. Wong, Algorithm AS 136: a K-means clustering algorithm, J. R. Stat. Soc. 28 (1979) 100–108, https://doi.org/10.2307/2346830.

[30] K.J. Hemker, B.G. Mendis, C. Eberl, Characterizing the microstructure and mechanical behavior of a two-phase NiCoCrAlY bond coat for thermal barrier systems, Mater. Sci. Eng. A 483–484 (2008) 727–730, https://doi.org/10.1016/j.msea.2006.12.169.

[31] J. Jiang, Z. Zou, W. Wang, X. Zhao, Y. Liu, Z. Cao, Effect of internal oxidation on the interfacial morphology and residual stress in air plasma sprayed thermal barrier coatings, Surf. Coat. Technol. 334 (2018) 215–226, https://doi.org/10.1016/j.surfcoat.2017.11.040.

[32] N.P. Padture, Thermal barrier coatings for gas-turbine engine applications, Science 296 (2002) 280–284, https://doi.org/10.1126/science.1068609.

[33] K.S. Chan, A mechanics-based approach to cyclic oxidation, Metall. Mater. Trans. A Phys. Metall. Mater. Sci. 28 (1997) 411–422, https://doi.org/10.1007/s11661-997-0142-2.

[34] C.J. Li, H. Dong, H. Ding, G.J. Yang, C.X. Li, The correlation of the TBC lifetimes in burner cycling test with thermal gradient and furnace isothermal cycling test by

TGO effects, J. Therm. Spray Technol. 26 (2017) 378–387, https://doi.org/10.1007/s11666-017-0530-0.
[35] J. Toscano, R. Vaßen, A. Gil, M. Subanovic, D. Naumenko, L. Singheiser, W.J. Quadakkers, Parameters affecting TGO growth and adherence on MCrAlY-bond coats for TBC's, Surf. Coat. Technol. 201 (2006) 3906–3910, https://doi.org/10.1016/j.surfcoat.2006.07.247.
[36] J.R. Brandon, R. Taylor, Phase stability of zirconia-based thermal barrier coatings part I. Zirconia-yttria alloys, Surf. Coat. Technol. 46 (1991) 75–90, https://doi.org/10.1016/0257-8972(91)90151-L.
[37] K.H. Schwalbe, On the influence of microstructure on crack propagation mechanisms and fracture toughness of metallic materials, Eng. Fract. Mech. 9 (1977) 795–832, https://doi.org/10.1016/0013-7944(77)90004-2.
[38] Z. Liu, W. Yan, S. Wolff, C. Yu, J. Cao, S. Lin, W.K. Liu, Y. Lian, G.J. Wagner, O.L. Kafka, Modeling process-structure-property relationships for additive manufacturing, Front. Mech. Eng. 13 (2018) 482–492, https://doi.org/10.1007/s11465-018-0505-y.
[39] P. Enrique-Jimenez, S. Quiles-Díaz, H.J. Salavagione, J.P. Fernández-Blázquez, M.A. Monclús, R. Guzman de Villoria, M.A. Gómez-Fatou, F. Ania, A. Flores, Nanoindentation mapping of multiscale composites of graphene-reinforced polypropylene and carbon fibres, Compos. Sci. Technol. 169 (2019) 151–157, https://doi.org/10.1016/j.compscitech.2018.11.009.
[40] Y. Chen, H. Kou, L. Cheng, Y. Zhang, Y. Yu, Y. Lu, Kinetic diffusion couple for mapping microstructural and mechanical data on Ti-Al-Mo titanium alloys, Materials (Basel) 11 (2018)https://doi.org/10.3390/ma11071112.
[41] S.R. Kalidindi, Hierarchical Materials Informatics, 2015.
[42] X. Li, Z. Liu, S. Cui, C. Luo, C. Li, Z. Zhuang, Predicting the effective mechanical property of heterogeneous materials by image based modeling and deep learning, Comput. Methods Appl. Mech. Eng. 347 (2019) 735–753, https://doi.org/10.1016/j.cma.2019.01.005.
[43] Z. Yang, Y.C. Yabansu, D. Jha, W. keng Liao, A.N. Choudhary, S.R. Kalidindi, A. Agrawal, Establishing structure-property localization linkages for elastic deformation of three-dimensional high contrast composites using deep learning approaches, Acta Mater. 166 (2019) 335–345, https://doi.org/10.1016/j.actamat.2018.12.045.